Int. J. Microgravity Sci. Appl., 34 (1) (2017) 340116
DOI: 10.15011//jasma.34.340116

IIIII ISPS-6 Proceedings IIIII
(Original Paper)

Growth and Characterization of Doped Ge Crystals under µg and 1 G to Investigate the Influence of Different Convection Types

Tina SORGENFREI [1], Adam HESS [1], Jan ZÄHRINGER [1], Andreas DANILEWSKY [1], Arne CRÖLL [1], Alexander EGOROV [2] and Alexander SENCHENKOV [2]

Abstract

Three Bridgman growth experiments were performed during the FOTON M4 mission in 2014. The aim of these experiments was to determine the influence of different convective states within the melt volume on the properties of the growing crystal. Transitions between different melt flow regimes were enforced during the ongoing growth by the application of rotating magnetic fields of different strengths and vibrations of different amplitude. A significant influence of the melt flow conditions on the Ga incorporation in the Ge crystal was observed for the µg crystals. The 1 G reference crystals, grown as well in the POLIZON 2 furnace (flight model) with the same parameters, showed always the expected dopant distribution as predicted by Scheil for complete mixing conditions. The buoyancy convection dominates the melt convection induced by the different RMFs or vibrations. The crystals were investigated by Differential Interference Contrast microscopy after structural etching, synchrotron topography to determine the structural quality, and spatially resolved resistivity measurements to determine the axial Ga segregation.

Keyword(s): Germanium, Doping, Bridgman growth, Melt growth, Convection, Diffusion, Segregation, Rotating magnetic field, Axial vibrations

Received 23 December 2015, Accepted 20 December 2016, Published 31 January 2017

1. Introduction

The requirements for semiconducting materials used in various applications in the fields of electronic devices and detectors rise constantly. Mostly these semiconductor crystals are produces by melt growth techniques. The influence of convective flows in the melt and capillary phenomena, i.e. wetting behavior, on the resulting crystal quality becomes more and more important to understand. Microgravity (µg) is a very important tool to investigate these effects. It allows the establishment of controlled and defined convective states because the influence of buoyancy convection is reduced significantly. The aim of this work is the investigation of actively influencing the structural and electric properties of semiconductor crystals during melt growth. This refers on the one hand to the active control of microscopic and macroscopic segregation of dopants and impurities, and on the other hand to the structural improvement (dislocation density, mechanical stress, inclusions). A series of Bridgman growth experiments was performed under different melt flow conditions by using external rotating magnetic fields of various strengths and vibrations of different amplitudes. Microgravity was used to separate the different melt flow states in semiconductor melts from buoyancy convection. Thus, the influence of the different melt flows on the structural, physical and chemical properties can be investigated and determined. The following melt flow states were investigated:

1. nearly diffusive conditions
2. laminar melt flow
3. time-dependent melt flow

Those three flow states were achieved by either using µg and/or by applying rotating magnetic fields of different strength. Two growth experiments were performed to investigate these flow states and the transitions between them. The experiment K1 investigated the transition between nearly diffusive conditions and laminar flow. The experiment K2 investigated the transitions from laminar flow to time-dependent convection and back. Additionally, experiments under vibrations with various amplitudes were performed to investigate their influence on segregation and interface curvature (experiment K3).

To achieve µg conditions, the experiments were performed during the FOTON M4 mission in summer 2014. The FOTON M4 satellite provided about 2 months overall experimental time with an orbital period of approx. 93 minutes[1)].

1 Crystallography, University of Freiburg, Hermann-Herder-Str. 5, 79104 Freiburg, Germany.
2 NIISK, Research and Development Institute for Launch Complexes, Moscow, Russia
(E-mail: tina.sorgenfrei@fmf.uni-freiburg.de)

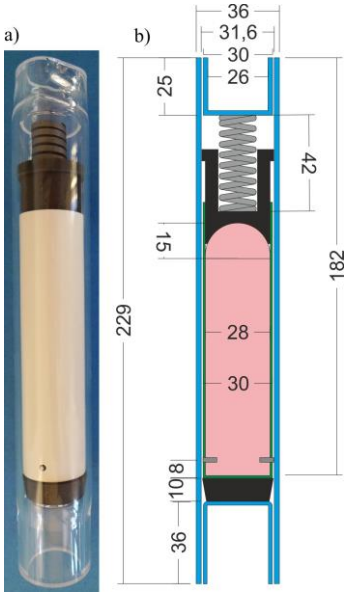

Fig. 1 a) Photograph of K1/K2 ampoule, b) schematic drawing of K1/K2 ampoule with measures in mm (explanation of single ampoule parts see text).

2. Experiments

2.1 Bridgman Furnace

For the Bridgman growth experiments on FOTON M4, and also the 1 G reference experiments, the POLIZON 2 furnace was used. This is a vacuum furnace with 4 heating zones in the Bridgman setup. Due to the fact that FOTON M4 was an unmanned mission, an automated cartridge exchange with a maximum cartridge diameter of 42 mm was implemented. Therefore, a maximum ampoule diameter of 36 mm was available. Additionally, rotating magnetic fields (RMF) of different strengths and frequencies could be applied. The sample temperature was controlled by 4 thermocouples located directly at the outer wall of the ampoules at different positions.

2.2 Sample Setup

The setup of the ampoules for the different experiments was similar. Despite the additional parts for vibration, the crucible part of the growing crystals built for K1, K2, and K3 was the same. **Figure 1** shows a photograph (a) and a schematic drawing (b) of the ampoules for the rotating magnetic field experiments (K1/K2).

Ga-doped Ge (pink) was used as seed and feed material. The advantage of using the same material for seed and feed is that the control of the position of the first phase boundary is less critical. The Ge seed was fixed by two Ta pins (grey) in a pBN (pyrolytic boron nitride) crucible (green). The Ge rod was

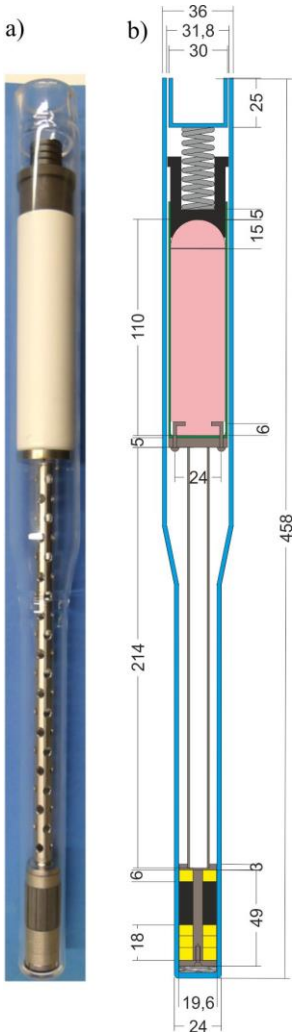

Fig. 2 a) Photograph of a K3 ampoule, b) schematic sketch of a K3 ampoule with measures in mm.

covered by a graphite plug (black). Because of the volume shrinkage of Ge while melting and to avoid free surfaces, and therefore prevent Marangoni convection, a CFC (carbon fiber carbon composite) spring was implemented to push the plug downwards and stay in contact with the melt all the time. The initial tension was adjusted such that it was strong enough to allow for the maximum volume shrinkage, but weak enough to prevent a spilling of melt out of the crucible. If liquid Ge gets in contact to the fused silica ampoule, the ampoule might crack. This setup was then sealed in evacuated fused silica ampoules (blue parts in fig. 1b, measures in mm).

The vibration source for the K3 ampoules consists of two parts: the first parts are strong Sm_2Co_{17} magnets (yellow in fig. 2b) located directly within the ampoule and connected to the crucible. The second part is an outer coil which was placed around the outer ampoule wall close to the inner magnets. Due to the transition temperature of the Sm_2Co_{17} magnets at about

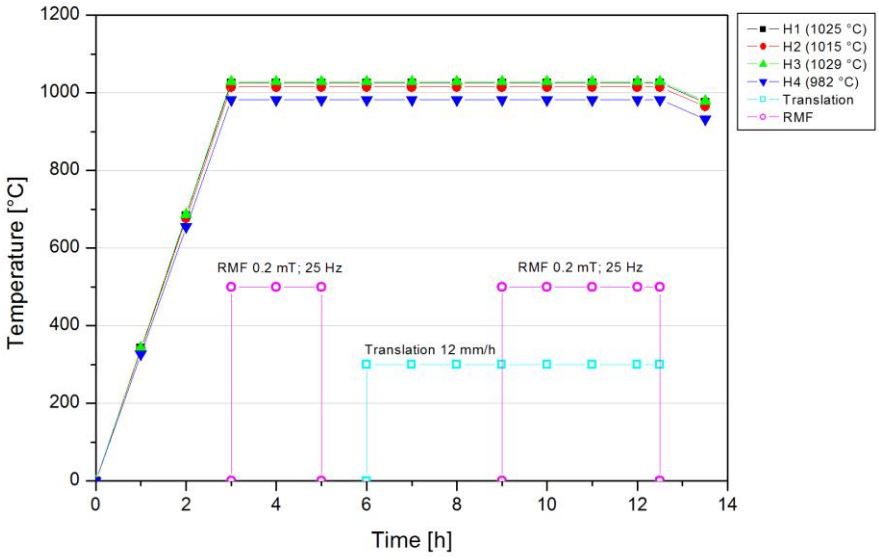

Fig. 3 Timeline of K1 experiment, the temperatures of the 4 heaters, the RMF and the translation are given.

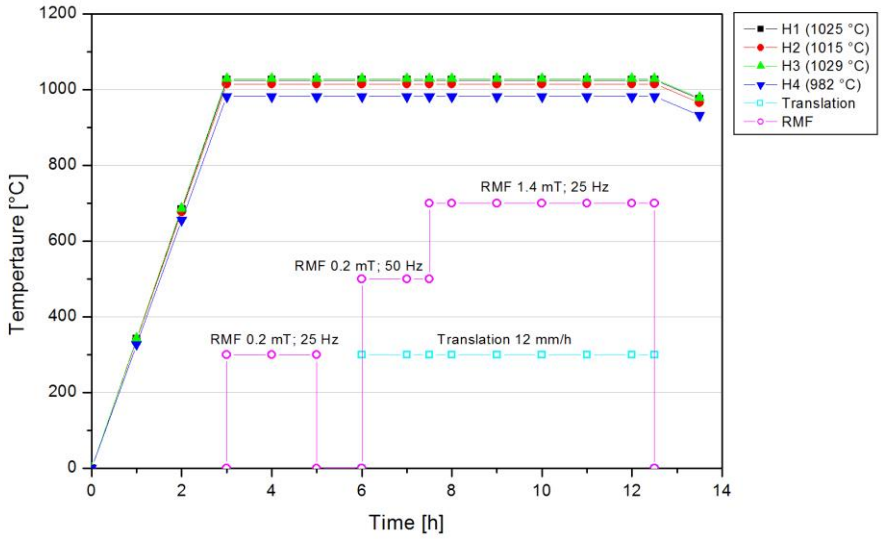

Fig. 4 Timeline of K2 experiment

300 °C a certain distance of the magnets to the hot zone had to be maintained. Therefore, a titanium tube of 250 mm length was connected to the crucible and the magnets were located at the other end of the tube. A photograph and a schematic sketch of a K3 ampoule are shown in **Fig. 2**.

In the lower part of fig 2b four Sm_2Co_{17} magnets are shown. Three magnets were used to trigger the vibration. A fourth Sm_2Co_{17} magnet located ca. 20 mm above the three driving magnets is oppositely polarized and acts as measuring magnet to get information about the real amplitudes during the growth. To reduce the heat flow towards the magnets several holes were drilled into the Ti tube.

2.3 Experiment Performance

To achieve the highest possible amount of information from the experiments, suitable timelines had to be chosen, identical for the µg and 1 G reference experiments. The reference experiments were also performed in the POLIZON 2 flight furnace on the ground in Moscow after the landing of FOTON M4 in September 2014.

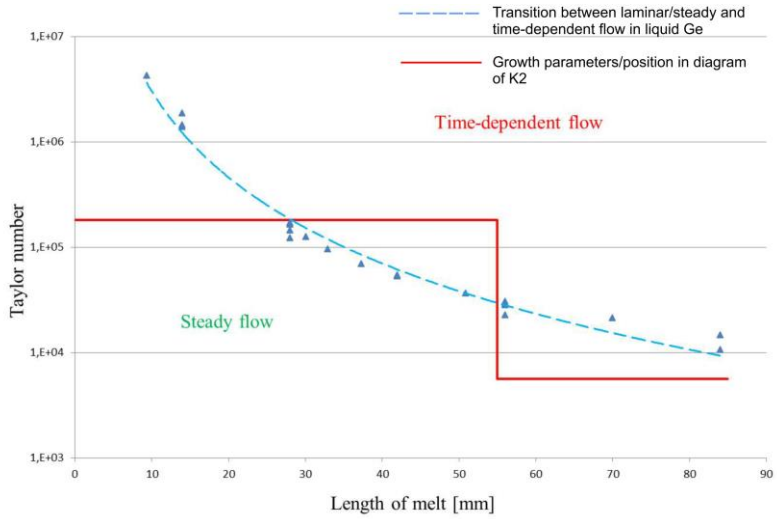

Fig. 5 Dependence of Taylor number and the length of melt calculated for a cylindrical melt volume with a diameter of 28 mm. Transition between laminar flow and time-dependent flow is shown as blue dashed line. The red solid line represents the growth parameters of K2 and the movement through the diagram.

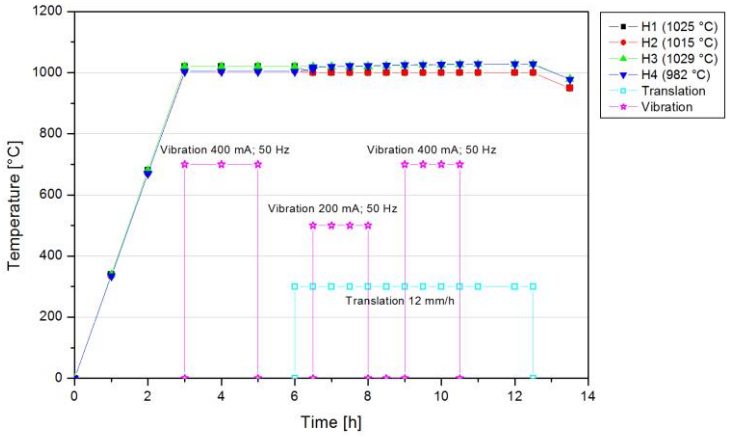

Fig. 6 Timeline of the K3 experiment using vibrations for homogenization and applying two stages of vibrations with different amplitudes during growth.

2.3.1 K1 Experiment

Figure 3 shows the timeline of the K1 experiment. The heating ramp was chosen in such a way that the final temperatures of all 4 heaters (between 982 and 1029 °C) were achieved after 3 hours. Immediately after complete melting and stabilization of the temperatures a weak RMF of 0.2 mT and 25 Hz was switched on for 2 h to homogenize the melt. After a subsequent 1 h of passive temperature equilibration without field, nearly diffusive conditions within the melt are ensured and the translation was started. Due to slight undercooling effects the growth started shortly after that. The translation speed and therefore the average growth velocity were 12 mm/h. After 3 h of crystal growth an RMF of 0.2 mT and 25 Hz was switched on to establish a laminar flow within the residual melt volume. After additional 3 h of crystal growth under laminar flow conditions the RMF and the translation were switched off and the growth stopped. For 1h the sample was cooled controlled; after that the heaters were switched off too.

2.3.2 K2 Experiment

The timeline of the K2 experiment (shown in **Fig. 4**) is the continuation of the K1 timeline. After the same heating and homogenization program the translation started again with 12 mm/h. Directly at the beginning of the growth an RMF with 0.2 mT and 50 Hz was applied to establish again a laminar flow state. Here a higher frequency was chosen. After 2 h of crystal

growth the parameters of the RMF were increased to 1.4 mT at 25 Hz to establish a time-dependent flow. With decreasing melt volume the flow state should go back to laminar flow conditions within the last part of this experiment. The dependence of the convective state (dependent on the critical Taylor number) and melt height (calculated for a cylindrical melt volume with a diameter of 28 mm) is given in **Fig. 5**.

2.3.3 K3 Experiment

In K3 the same temperature program as for K1 and K2 was applied, but no RMF was used (neither for homogenization nor for the control of the flow state). Instead of the RMF the whole pBN crucible, and therefore seed and melt were vibrated. The timeline for this experiment is shown in **Fig. 6**. Similar to K1 and K2, after heating up a homogenization step of 2 h was implemented. Therefore, the vibration coil was driven with 400 mA and 50 Hz, this led to an amplitude of ca. 260 µm which equals an acceleration of 1.3 G. Before the translation started, 1 h of equilibration time without vibrations was used. After that, 30 minutes of growth under microgravity conditions were performed, then the first stage of vibrations with 200 mA and 50 Hz was started. These values resulted in an amplitude of ca. 170 µm and an acceleration of about 0.88 G. This vibration state was held for 90 min. Then the vibration was switched off for duration of 1h before the second vibration stage with 400 mA at 50 Hz for again 90 min was started. Afterwards, the vibration was switched off and the growth proceeded for additional 2 h. Then the translation was switched off and the growth stopped. At the end, the controlled cooling continued for 1 h and the heaters were switched off.

2.3.4 Sample Preparation

After a visual inspection of the processed ampoules to check for damages which might have influenced the crystal growth, the ampoules were disassembled. The different parts of the ampoules were also checked with respect to damage or visible traces of chemical or physical interactions. In all cases, the crystals could be removed from of the pBN crucibles without difficulty. After a detailed inspection and documentation of the crystal surface all crystals were cut into axial slices by an inner diameter saw. **Figure 7** shows the K1 µg sample a) after being processed, b) the processed and disassembled crystal, and c) the as-cut slices. All samples (µg and 1 G) were prepared this way. The slices were polished on both sides and etched to delineate striations. These striations originate from micro segregation effects of the dopant (Ga) and can be used to determine the exact growth velocity at certain points. The analysis of the samples was done by profilometer measurements (to determine the thickness of the gap that appeared between growing crystal and crucible inner wall due to so-called detached growth), DIC microscopy, resistivity measurements, and X-ray topography.

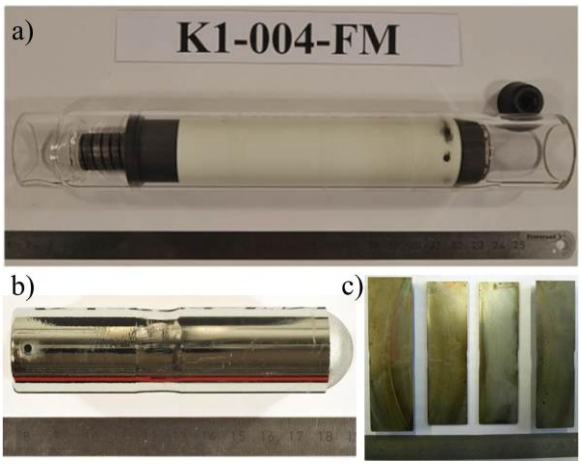

Fig. 7 K1 µg sample a) complete ampoule removed from the cartridge after the experiment, b) the whole crystal, c) crystal cut into slices by an inner diameter saw for further preparation and characterization.

3. Results

All experiments were performed without difficulties during or after growth. All ampoules were in good condition without any cracks or visible damages. Thus, all crystals could be prepared as described in chapter 2.3.4.

3.1 K1 Experiments

Figure 8 shows the µg crystal (a) and the 1 G reference crystal (b) before preparation. The µg crystal exhibits a 14 mm long part with smaller diameter in the middle of its cylindrical shaped body. This originates from so-called detached growth[2-4]. In this case, the growing crystal and a small melt meniscus have no contact to the crucible wall.

Detached growth leads in principle to a reduced number of defects. Detached Bridgman growth was primarily observed in previous µg experiments, but is not fully limited to these

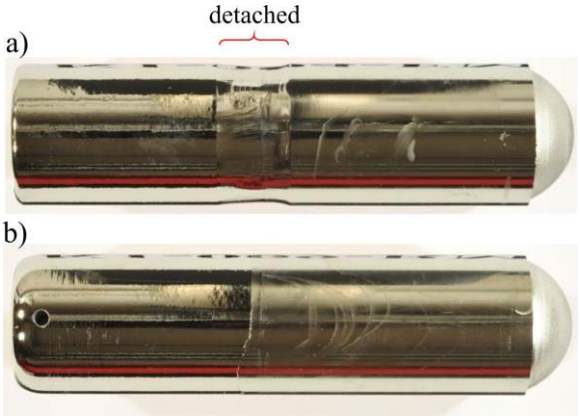

Fig. 8 Photograph of a) the K1 µg crystal with a detached grown area at the beginning of the growth for about 14 mm and b) the 1 G reference crystal which grew completely attached.

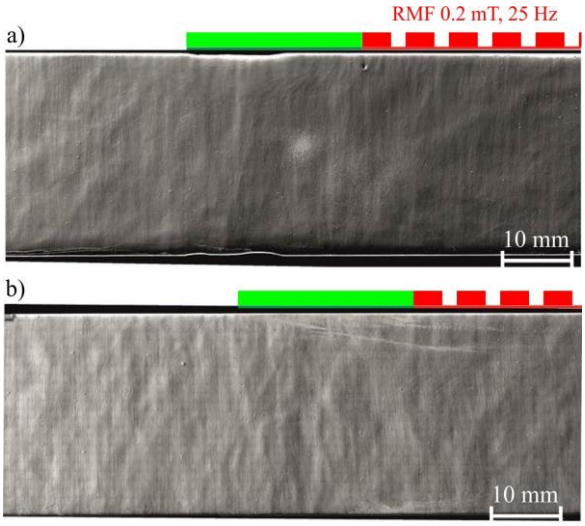

Fig. 9 DIC images of the etched a) µg K1 sample and b) 1 G reference sample. The green lines above the images represent the diffusive regime, the red dashed line represents the growth under laminar flow.

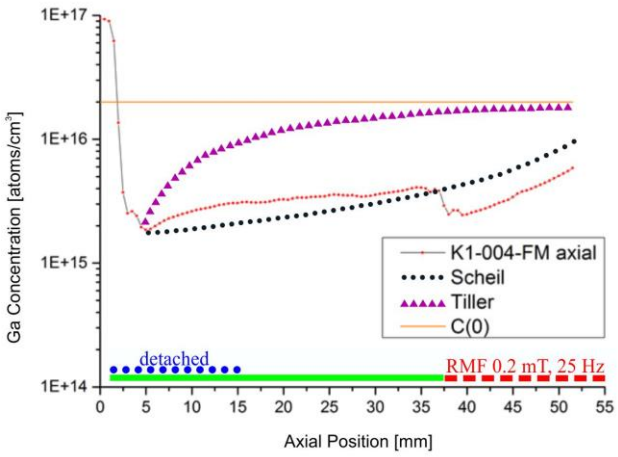

Fig. 10 Ga concentration in dependence of the axial position of the K1 µg crystal, determined by spatially resolved resistivity measurements. The green line represents the mostly diffusive growth regime, the dashed red line represents the laminar flow state.

conditions. There are several publications dealing with the investigation of detached growth, but controlled detachment is hard to achieve[2-4]. A very interesting point for the K1 µg crystal is that the detached growth appeared despite the pressure from the CFC spring on the melt. The best explanation is that the graphite plug got stuck at some point during the melting process. Without a spring, the detached growth might have continued over even a longer distance. Due to the melt meniscus, which has formed between crystal and crucible, a free melt surface was generated. Thus, for a detailed analysis, a slight contribution of localized Marangoni convection has to be taken into account.

3.1.1 Differential Interference Contrast Microscopy

Figure 9 shows DIC microscopy images of the etched sample slices of the K1 µg (a) and the 1 G reference crystal (b). The green line above both images represents the growth distance under nearly diffusive conditions and the red dashed line the growth under laminar flow. The laminar flow was induced by a RMF of 0.2 mT at 25 Hz.

Both samples are single crystalline, but no dopant striations are visible. Due to this, an exact determination of the real growth velocity cannot be made at this point. In fig. 9a the detached growth can also be observed due to the reduced diameter of the slice. In contrast, the 1 G crystal was grown completely attached.

3.1.2 Segregation Analysis

Spatially resolved resistivity measurements were done to determine the axial segregation in the Ga-doped Ge crystals. **Figure 10** shows the plotted Ga concentration obtained from the resistivity measurements in dependence of the axial position. Due to a segregation coefficient of 0.087 of Ga in Ge [5], the interface between seed and grown crystal appears as a sharp decrease of the Ga concentration. The growth distance under nominally diffusive conditions is shown by the green line at the bottom of the diagram; the red dashed line represents the laminar flow regime. The detached grown crystal part is indicated by the blue dotted line at the diagram bottom. The average Ga concentration was calculated to be $2x10^{16}$ at/cm^3 and is drawn as solid orange line in **Fig. 10**. The seed part was doped higher than the feed part to ensure the visibility of the first S/L interface, therefore, the concentration curves starts above $2x10^{16}$ at/cm^3.

The µg crystal shows mostly diffusive behavior in the detached region. With the beginning of the attached growth small fluctuations appear, but still diffusive conditions define the growth regime. The deviation from the segregation after Tiller [6] (grey dotted fit) for pure diffusive conditions may be caused by the light melt flow due to Marangoni convection and possibly some residual gravity driven convection[7,8]. At the moment when the RMF was switched on, the slope of the segregation curve changes significantly. The Ga concentration decreases and the slope of the remaining curve follows - with a small difference - the Scheil equation which describes segregation in a completely mixed regime[9].

The result of the segregation analysis of the 1 G reference crystal is shown in **Fig. 11**. Similar to the diagram in **Fig. 10**, the part grown without RMF is represented by the green solid line and the part with RMF (0.2 mT and 25 Hz) is represented by the dashed red line at the bottom of the data plot. The interface between seed and grown crystal can be observed due to the sharp decrease of the Ga concentration at the axial position of ca. 5 mm. The whole segregation curve follows in its

slope the theoretical curve for complete mixing conditions after Scheil (grey dotted fit). No change in the Ga concentration at the switching point of the RMF can be observed. Thus, the buoyancy convection dominates the melt flow during the whole experiment. This shows that the influence of the buoyancy convection driven by the gravitational force is much stronger than the influence of a RMF of the strength applied here.

3.1.3 Synchrotron Topography

To compare the dislocation densities of the crystals grown under µg and 1 G conditions synchrotron topography measurements in the back reflection mode were performed[10]. The pictures of these measurements are not shown here, but a reduced dislocation density of at least one order of magnitude was measured for the µg crystal compared to the 1 G reference. While the 1 G reference crystal shows a dislocation density of $5x10^4$ cm^{-2}, the µg crystal exhibits only $3x10^2$ to $5x10^3$ dislocations per cm^2, which can be attributed to the initial detached growth regime. The higher values for the µg crystal are located in the attached grown regions.

3.2 K2 Experiments

3.2.1 Differential Interference Contrast Microscopy

Figure 12 shows the DIC images for the µg (a) and the 1 G reference (b) K2 crystals. The red line represents the length of the crystal which was grown under laminar flow conditions induced by a RMF with 0.2 mT and a frequency of 50 Hz. The purple dashed line represents the crystal length which was grown under an RMF of increased strength. The parameters were chosen in such a way that at the beginning of this second part time-dependent melt flow should occur. Due to the constant decrease of melt height during growth, the Taylor number for the applied RMF should go below the critical value. Thus, the growth conditions will go back to a laminar flow regime. Similar to the K1 samples and despite the inserted CFC spring, in the µg experiment detached growth occurred up to a maximum length of 12.1 mm. Especially at the lower edge of the slice in **Fig. 12a** the lower diameter due to detachment can be observed. A maximum gap thickness of 500 µm was measured by a profilometer. The 1 G crystal grew again completely attached. Also similar to the K1 samples, no striations could be delineated by etching. But both samples are single crystalline, no grain or twin boundaries are observable.

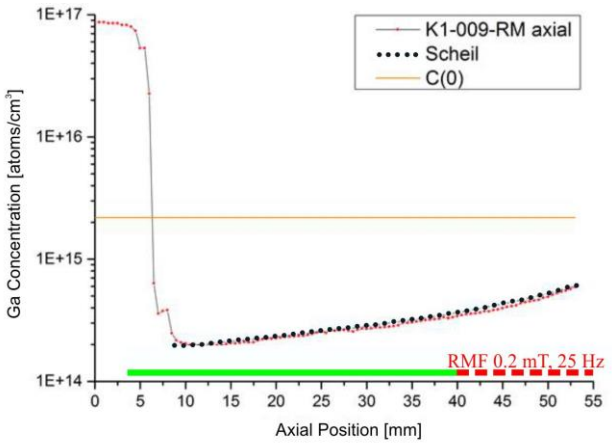

Fig. 11 Segregation profile of the K1 1 G reference crystal.

3.2.2 Segregation Analysis

In case of the K2 experiments the Ga incorporation was similar for the µg and the 1 G crystal. The plotted data of the Ga concentration obtained from the resistivity measurements are shown in **Fig. 13**. Similar to **Fig. 12** the first stage of the weaker RMF is represented by the red line and the stronger RMF, applied during the second stage, is represented by the purple dashed line. Additionally, the maximum detached length is given by the blue dotted line.

Both, the µg (**Fig. 13a**) and the 1 G (**Fig. 13b**) crystals show a similar overall behavior. The slopes of the Ga incorporation curves can be described by the Scheil equation. There is a small deviation from the Scheil fit for the µg crystal during the first stage of RMF. Similar to the K1 µg experiment, fluctuations in the Ga concentration can be observed during the detached growth. The origin of these deviations cannot be explained at the moment. An additional similarity of the µg and the 1 G crystal is the drop of Ga concentration directly at the switching point of the RMF. A possible explanation for this phenomenon is the increased mixing. The fact that no striations were visible in

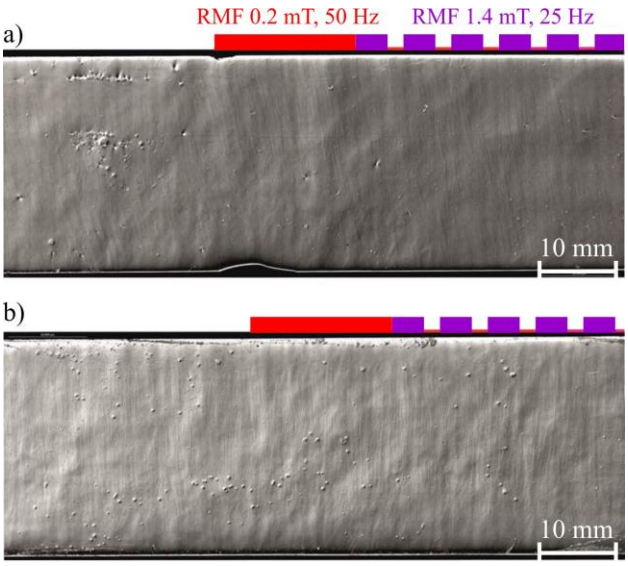

Fig. 12 DIC images of the etched a) µg K2 sample and b) 1 G reference sample. The red lines above the images represent the laminar flow regime induced by a RMF of 0.2 mT and 50 Hz, the purple dashed line represents the growth with an applied RMF of 1.4 mT and 25 Hz. Due to the decrease of melt volume, a transition from time-dependent flow back to laminar flow occurred during this part.

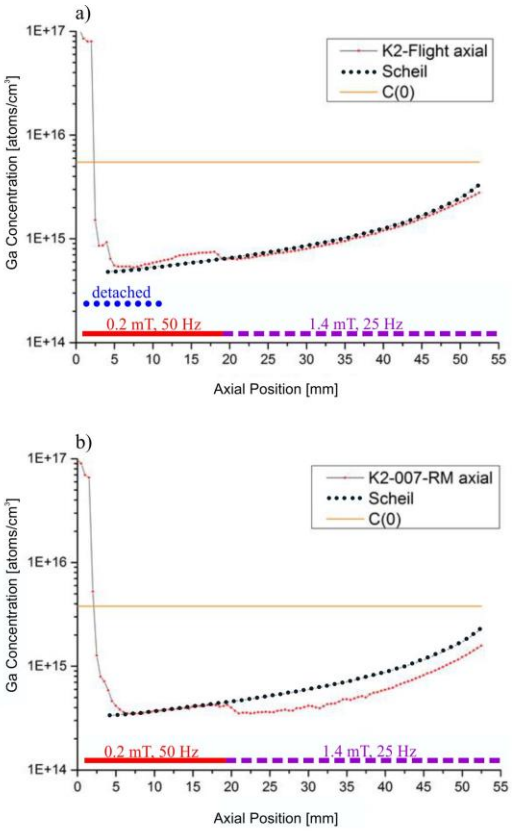

Fig. 13 Segregation profiles of a) the µg crystal and b) the 1 G reference crystal of the K2 experiments. The corresponding Scheil fit is plotted as grey dotted line.

the etched crystals, could point to a non-time-dependent flow regime over the whole crystal. Further analysis will be done to clarify this point.

3.2.3 Synchrotron Topography

For the K2 experiments the dislocation density of the µg sample within the crystal part grown at the first stage of RMF was determined by synchrotron topography measurements [10]. The measured values range between $2x10^2$ and $8x10^3$ cm^{-2} and correspond to the dislocation densities of the detached and the attached grown crystal parts, respectively. The number of dislocations is slightly increased compared to the K1 µg crystal; this might be caused by the shorter detached growth.

3.3 K3 Experiments

3.3.1 Differential Interference Contrast Microscopy

Figure 14 shows the DIC images of the K3 crystals. In fig. 14a an etched slice of the µg sample and in 14b an etched slice of the 1 G reference sample are shown. Due to the same low dopant concentration as for the crystals of K1 and K2, also in K3 no striations are visible after etching. While the 1 G sample is single crystalline, the µg became polycrystalline on one side

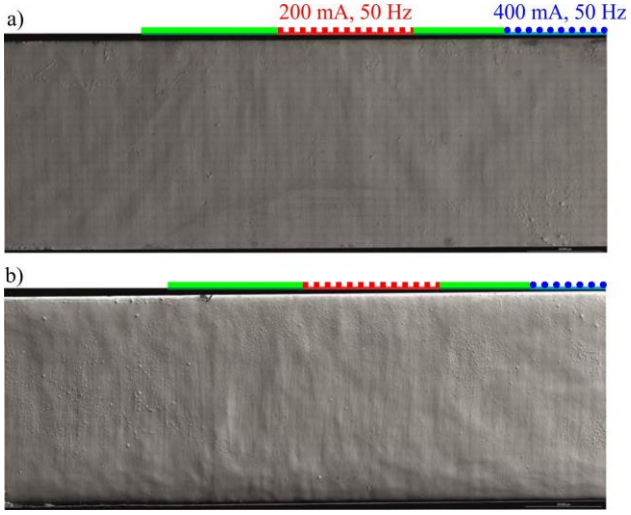

Fig. 14 DIC images of a) the etched K3 µg slice and b) the etched K3 1 G slice. The µg sample exhibits a polycrystalline part, starting from the lower edge near the first phase boundary.

directly at the beginning of the growth (see **Fig. 14a**, lower crystal edge). The origin of the polycrystalline growth cannot be determined, but in all probability a particle of or on the crucible inner wall was responsible for heterogeneous seeding and the resulting off-oriented growth.

3.3.2 Segregation Analysis

The concentration of the incorporated Ga in the K3 1 G sample follows the theoretical predictions by Scheil for complete mixing (see **Fig. 15**). The measured and the calculated values are in very good agreement. This shows that the vibration induced states are completely dominated by the buoyancy convection.

The green solid lines at the bottom of the diagram represent the growth parts without any influence on the melt convection, i.e. no vibration and no RMF. The red dashed line shows the duration of the first vibration stage, the chosen parameters of 200 mA and 50 Hz resulted in an amplitude of about 170 µm. The blue dotted line represents the second vibration state with increased current (400 mA) at the same frequency of 50 Hz, this resulted in an amplitude of about 260 µm. Both vibration states did not influence the Ga incorporation.

A different behavior of the segregation can be observed in the µg sample of K3. The same parameters for vibration, growth, and duration were applied, but the slope of the Ga concentration differs drastically from that of the 1 G reference. The measured and theoretical values for the Scheil and the Tiller equation are shown in **Fig. 16**. Similar to **Fig. 15** the -under µg- mostly diffusive growth stages are represented by the green solid lines at the diagram bottom, the vibration stages with the lower and the higher amplitude by the red dashed and the blue dotted lines, respectively. The calculated values of the Scheil fit are plotted

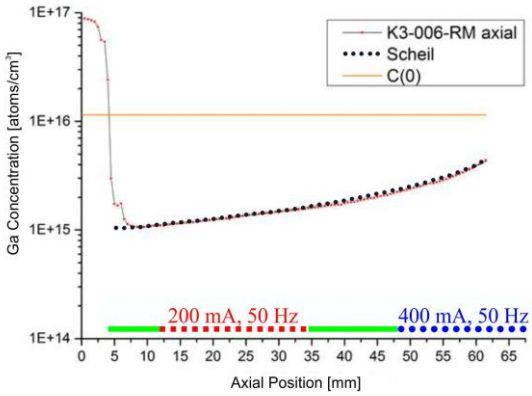

Fig. 15 Segregation profile of the K3 1 G reference crystal. The Ga concentration can be fitted exactly by the Scheil equation for complete mixing.

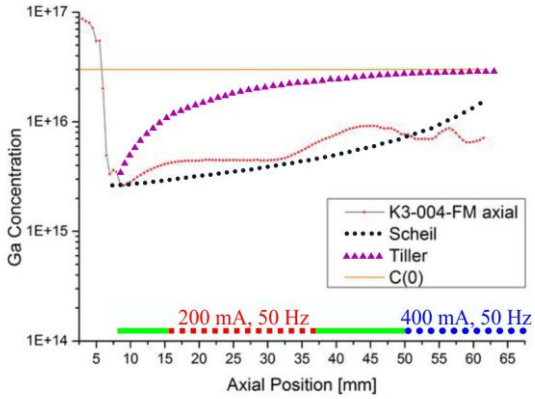

Fig. 16 Segregation profile of the K3 µg sample. The green lines represent the mostly diffusive growth regimes, the green dashed line and the purple dotted line represent the vibration states.

as grey dashed line and the ones of the Tiller fit as grey dotted line next to the measured values (red). The sharp drop in Ga concentration at the left side of the diagram corresponds to the first solid-liquid interface (due to k<<1).

During the first growth section under microgravity condition the amount of incorporated Ga follows a slope for mostly diffusive conditions with a certain deviation. During the second growth section the first set of vibrations was applied. Here, the slope of the Ga concentration curve is completely flat for the duration of the whole section. This means that the Ga incorporation was homogeneous during the vibrational growth. When the vibrations stopped, the system returned to the previous dopant incorporation behavior. Within all these three sections the slope of the Ga concentration curve is smooth. This undergoes a radical change with the start of the fourth section when the vibrations of higher amplitude were applied. Again, the incorporation behavior cannot be described by Scheil or Tiller, but it seems that the curve runs again into a (strongly fluctuating) linear slope with an inclination near 0 or slightly negative. To explain the different incorporation behaviors during the vibrations an additional kind of melt movement has to be taken into account. Vibration of a melt with a density gradient leads to a volume flow. In addition, the so-called Schlichting effect [11], originally described for aerodynamics, describes the appearance of a flow directly at a vibrating S/L interface for non-flat interfaces. Due to the occurrence of this melt flow directly within the diffusion boundary layer a significant influence on the segregation behavior is expected. Theoretical simulations to determine the influencing parameters as well as further quantitative investigations have to be done.

The K3 experiments show that vibrations have a significant influence on the phenomena directly at the growth front, but they are dominated by the buoyancy convection if grown in presence of gravity, at least for the amplitudes and frequencies employed here. The probability of the occurrence of foreign phase particles in the melt, originating from the crucible or other ampoule parts, is slightly increased if moving parts are used within the setup. But at this point, no influence of the vibrations on the structural quality can be observed.

4. Conclusions

All Bridgman growth experiments performed on FOTON M4 in the POLIZON 2 furnace were successful and yielded single crystalline material of high quality for analysis. Unexpected was the detached growth that appeared in the µg experiments of K1 and K2. Despite a permanent pressure upon the Ge melt, the system was able to form a melt meniscus between crucible and growing crystal and therefore a gap between grown material and crucible. Synchrotron topography measurements showed a significantly decrease of nearly two orders of magnitude of the dislocation density in case of detached compared to attached growth. The influence of the different triggered melt flow states (nearly diffusive conditions, laminar flow, and time-dependent flow) on the dopant incorporation behavior could be seen only in the µg samples. The different melt flow states were induced by RMFs of different strengths. An additional melt flow state was enforced by the appliance of vibrations. Two different amplitudes of 170 µm and 260 µm were applied. The weaker vibration led to a completely homogeneous dopant incorporation without any fluctuations during the whole growth section. To explain this phenomenon the so-called Schlichting effect has to be taken into account. During the stronger vibration section bigger fluctuations in the dopant concentration occurred.

Additional analysis will be performed and published later, i.e. LPS measurements to determine the exact growth velocities.

This might help to explain the different dopant concentration drops at several switching points; further synchrotron topography to determine spatially resolved dislocation densities and HRXRD measurements. Numerical simulations based on the actual flight parameters, including the µg disturbances, have started.

Acknowledgement

This work was funded by DLR/BMWi under FKZ 50WM1149. The authors thank C. Lehmann and M. Kranz-Probst for sample preparation. The assistance of the OHB team, especially Dr. P. Sickinger, during pre- and postprocessing the FOTON M4 mission is greatly appreciated.

References

1) URL: http://www.russianspaceweb.com/foton_m4.html, (2014) release date: 21.12.2015
2) A. Cröll and M.P. Volz: MRS Bulletin, **34 (4)** (2009) 245.
3) T. Duffar and L. Sylla: Crystal growth processes based on capillarity, Wiley, (2010) 355.
4) D. Langheinrich, O. Pätzold, J. Raabe and M. Stelter: J. Crystal Growth, **312** (2010) 229.
5) H.F. Hadamovsky (Ed.): Werkstoffe der Halbleitertechnik, VEB Deutscher Verlag für Grundstoffindustrie, Leipzig, (1990).
6) W.A. Tiller, K.A. Jackson, J.W. Rutter and B. Chalmers: Acta Metal, **1** (1953) 428.
7) G.. Ostrogorsky and G . Müller: J. Crystal Growth, **128** (1993) 207.
8) J.P. Garandet, S. Corre, S. Kaddeche, T. Alboussiere: J. Crystal Growth, **209** (2000) 270.
9) E. Scheil: Z. Metallk, **34** (1942) 70
10) A.N. Danilewsky, R. Simon, A. Fauler, M. Fiederle and K.W. Benz: Nuclear Instruments and Methods in Physics, B **199(1)** (2003) 71.
11) H. Schlichting and K. Gersten: Grenzschicht-Theorie. 10th Edition, Springer, (2006).